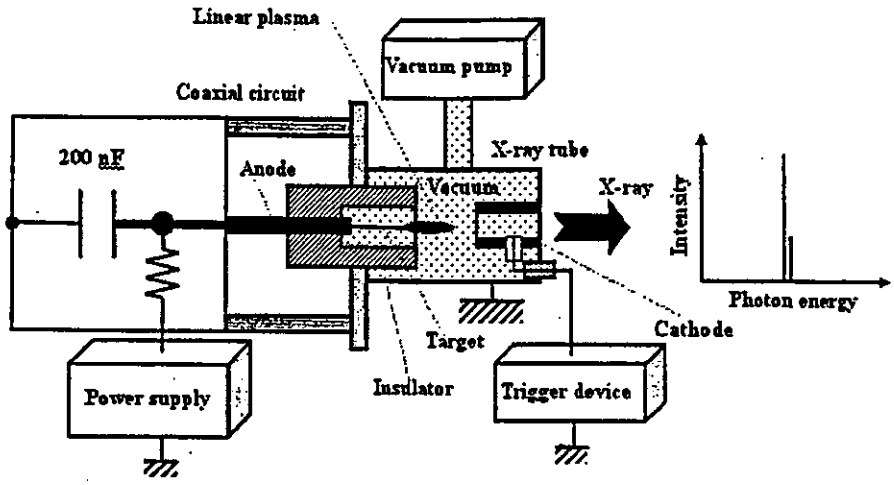

Fig. 1 . Block diagram of the high-intensity plasma flash x-ray generator.

have been employed to perform microangiography [1] and phase imaging [2,3]. However, the synchrotrons consume high energies, and it is difficult to obtain sufficient machine times for medical diagnosis and other applications.

Currently, flash x-ray generators utilize cold-cathode radiation tubes and produce high-dose-rate x-rays [4-12]. Therefore, in order to produce fairly high-dose-rate monochromatic x-rays in a small laboratory, plasma flash x-ray generators are useful. Subsequently, we confirmed the irradiation of intense characteristic x-rays from the plasma axial direction using plate targets. Thereafter, we developed a new plasma flash x-ray tube with a rod-shaped target [15,16], and confirmed fairly intense and sharp characteristic x-rays such as lasers from weakly ionized linear plasma.

Photon energies of characteristic x-rays are determined by the target element, and characteristic x-rays from a cerium target are useful to perform angiography using an iodine-based contrast medium, since the photon energies of K-series lines of cerium are slightly higher than the energy of the K-absorption edge of iodine. On the other hand, cerium is a rare earth element and has a high reactivity, and it is difficult to design the target. However, the development of a cerium plasma tube for high-contrast angiography has long been wished for.

In this paper, we describe a singe flash x-ray generator for producing intense characteristic x-rays by forming weakly ionized linear plasma, used to perform quasi-monochromatic radiography.

2. GENERATOR

2.1 High-voltage circuit

Figure 1 shows a block diagram of a high-intensity plasma flash x-ray generator. This generator consists of the following essential components: a high-voltage power supply, a high-voltage condenser with a capacity of approximately 200 nF, a turbo-molecular pump, a krytron pulse generator as a trigger device, and a flash x-ray tube. In this generator, a low-impedance transmission line is employed in order to increase maximum tube current. The high-voltage main condenser is charged up to 55 kV by the power supply, and electric charges in the condenser are discharged to the tube after triggering the cathode electrode with the trigger device. The plasma flash x-rays are then produced.

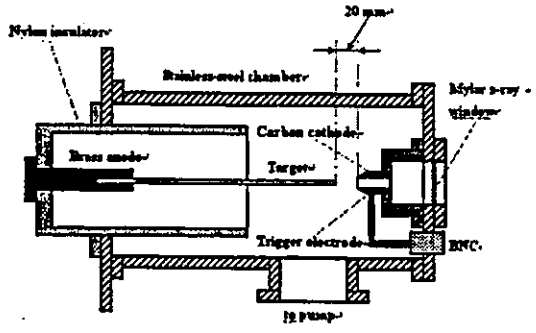

Fig. 2 Schematic drawing of the flash x-ray tube with a rod target.

2.2 X-ray tube

The x-ray tube is a demountable cold cathode triode that is connected to the turbo molecular pump with a pressure of approximately 1 mPa (Fig. 2). This tube consists of the following major parts: a pipe-shaped carbon cathode with a bore diameter of 10.0 mm, a trigger electrode made from copper wire, a stainless-steel vacuum chamber, a nylon insulator, a polyethylene terephthalate (Mylar) x-ray window of 0.25 mm in thickness, and a rod-shaped targets made of copper, molybdenum, and cerium. The diameters of copper, molybdenum, and cerium targets are 3.0, 2.0, and 3.0 mm, respectively. The distance between the target and cathode electrodes is approximately 20 mm, and the trigger electrode is set in the cathode electrode. As electron beams from the cathode electrode are roughly converged to the target by the electric field in the tube, evaporation leads to the formation of weakly ionized linear plasma, consisting of molybdenum ions and electrons, around the fine target.

2.3 Principle of characteristic x-ray irradiation

In the linear plasma, bremsstrahlung spectra with photon energies of higher than the K-absorption edge are effectively absorbed and are converted into fluorescent x-rays (Fig. 3). The plasma transmits the fluorescent rays easily, and bremsstrahlung rays with energies of lower than the K-edge are also absorbed by the plasma. In addition, because bremsstrahlung rays are not emitted in the direction opposite to electron acceleration, intense characteristic x-rays are generated from the plasma-axial direction.

3. CHARACTERISTICS

3.1 Tube voltage and current

Tube voltage and current were measured by a high-voltage divider with an input impedance of 1 GΩ and a current transformer, respectively. Figure 4 shows the time relation between the tube voltage and current obtained using a copper target. At the indicated charging voltages, they roughly displayed damped oscillations. When the charging voltage was increased, both the maximum tube voltage and current increased. At a

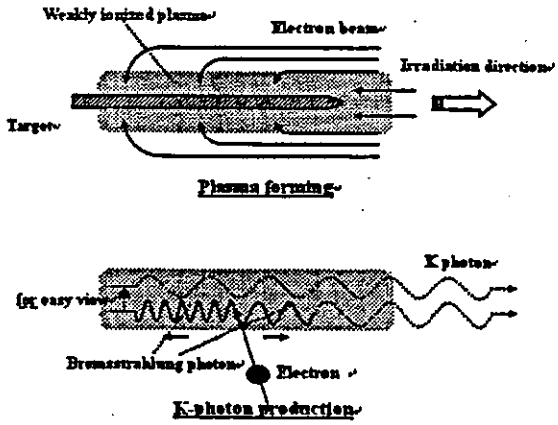

Fig. 3 K-photon irradiation from the plasma.

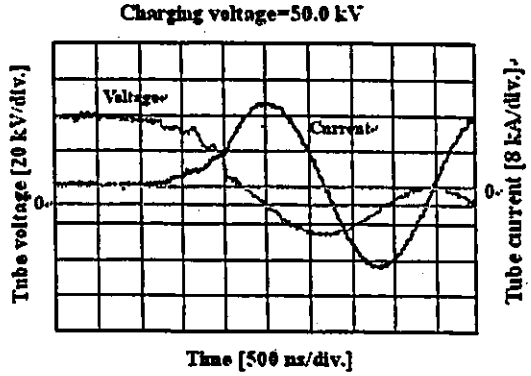

Fig. 4 Tube voltage and current obtained by a copper target with a charging voltage 50 kV.

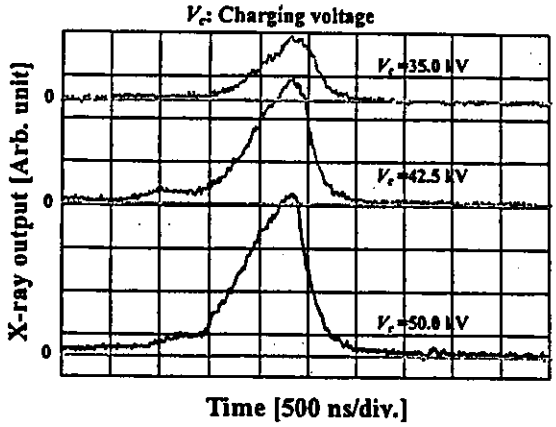

Fig. 5 X-ray outputs using a copper target.

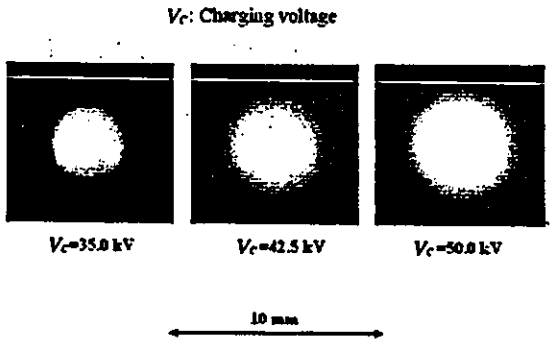

Fig. 6 Images of copper plasma x-ray source.

charging voltage of 50 kV, the maximum tube voltage was almost equal to the charging voltage of the main condenser, and the maximum tube current was approximately 20 kA.

3.2 X-ray output

X-ray output pulse was detected using a combination of a plastic scintillator and a photomultiplier. The x-ray pulse height substantially increased with corresponding increases in the charging voltage when the copper target was employed (Fig. 5). The x-ray pulse widths were about 700 ns, and the time-integrated x-ray intensity measured by a thermoluminescence dosimeter (Kyokko TLD Reader 1500 having MSO-S elements without energy compensation) had a value of about 30 μC/kg at 1.0 m from the x-ray source with a charging voltage of 50 kV.

3.3 X-ray source

In order to measure images of copper plasma x-ray source, we employed a pinhole camera with a hole diameter of 100 μm (Fig. 6). When the charging voltage was increased, the plasma x-ray source grew, and both

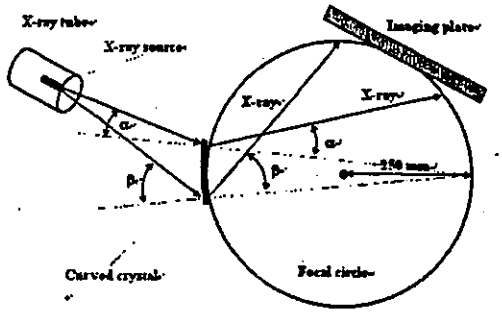

Fig. 7 Transmission-type spectrometer using an imaging plate.

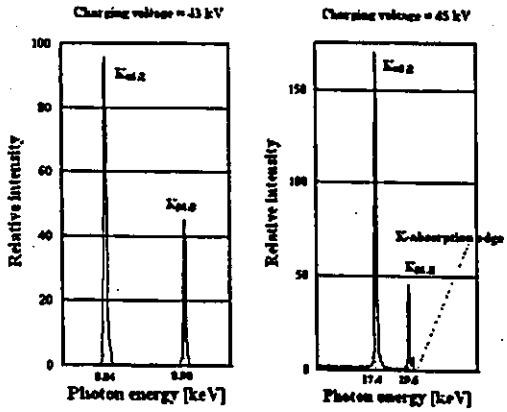

Fig. 8 X-ray spectra from weakly ionized copper and molybdenum plasmas.

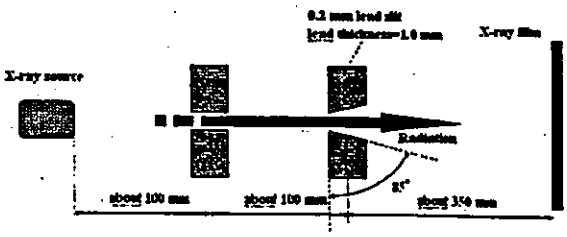

Fig. 9 Experimental setup for measuring x-ray divergence using two lead slits.

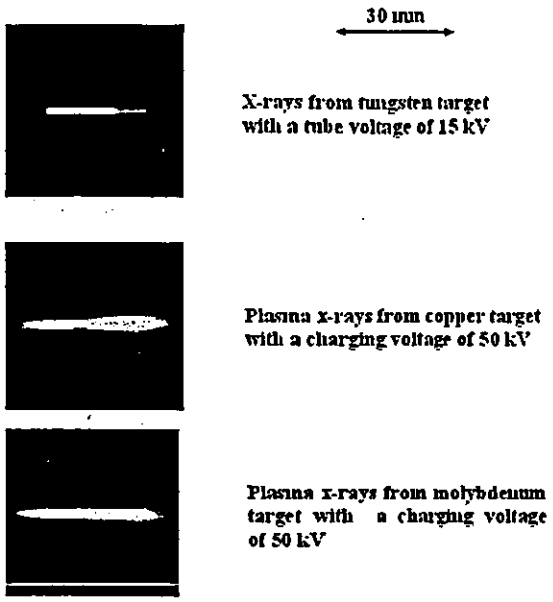

Fig. 10 X-ray divergence using copper and molybdenum targets.

spot dimension and intensity increased. In contrast, both the dimension and intensity decreased according to insertion of the monochromatic filter.

3.4 X-ray spectra

X-ray spectra from the plasma source were measured by a transmission-type spectrometer with a lithium fluoride curved crystal of 0.5 mm in thickness (Fig. 7). The spectra were taken by a computed radiography (CR) system [17] with a wide dynamic range, and relative x-ray intensity was calculated from DICOM digital data. Figure 8 shows measured spectra from the copper and the molybdenum targets. In fact, we observed quite sharp lines of K-series characteristic x-rays such as lasers, while bremsstrahlung rays were hardly detected. The characteristic x-ray intensity substantially increased with corresponding increases in the charging voltage and decreased with insertion of the filter.

3.5 X-ray diffraction by slits

In order to measure the difference in characteristics between x-rays from a conventional tube and these from the plasma tubes, we employed two lead slits in order to measure the divergence of the x-rays (Fig. 9). As compared with x-rays from a conventional tube with a tungsten target, the characteristic x-rays from linear plasmas of copper and molybdenum were diffused greatly after passing through the two slits (Fig. 10).

4. RADIOGRAPHY

The plasma radiography was performed by the CR system (Konica Regius 150) without using a monochromatic filter, and the distance between the x-ray source and imaging plate was 1.2 m. Radiograms

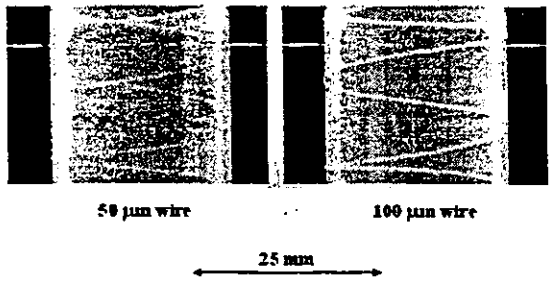

Fig. 11 Radiograms of tungsten wires 50 and 100 μm in diameter, respectively, coiled around pipes made of PMMA

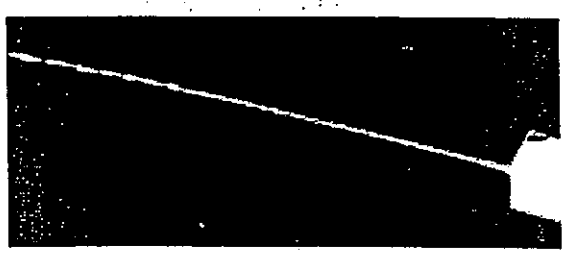

Fig. 12 Radiogram of water spouted from an injector.

Table 1 K-series characteristic x-rays of copper.

Line	Relative intensity	Photon energy (keV)
$K_{\alpha 1}$	100	8.046
$K_{\alpha 2}$	50	8.026
$K_{\alpha 1,2}$	150	8.040
$K_{\beta 1}$	6	8.901
$K_{\beta 1,3}$	20	8.904

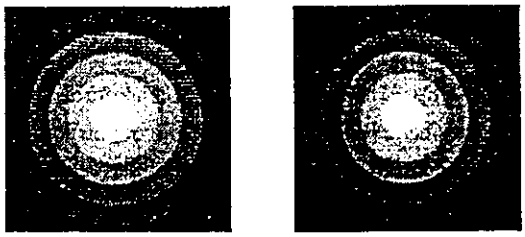

Fig. 13 Radiograms of concentric-circled steps of 5.0 mm made of PMMA with a maximum height of 25.0 mm.

Fig. 14 Angiogram of the external ear of a rabbit.

Table 2 K-series characteristic x-rays of molybdenum.

Line	Relative intensity	Photon energy (keV)
$K_{\alpha 1}$	100	17.476
$K_{\alpha 2}$	50	17.371
$K_{\alpha 1,2}$	150	17.441
$K_{\beta 1}$	17	19.605
$K_{\beta 3}$	7	19.587

Table 3 K-series characteristic x-rays of cerium.

Line	Relative intensity	Photon energy (keV)
$K_{\alpha 1}$	100	34.714
$K_{\alpha 2}$	50	34.273
$K_{\alpha 1,2}$	150	34.566
$K_{\beta 1}$	22	39.251
$K_{\beta 3}$	10	39.163

achieved with a copper target (Table 1) with a charging voltage of 50 kV are shown in Figs. 11 and 12. Figure 11 shows radiograms of tungsten wires coiled around pipes made of polymethyl methacrylate (PMMA). The image contrast of a 50 μm-diameter wire around pipe was lower than that of 100 μm wire, and the wires were almost completely visible. Next, the image of water spouted from an injector is shown in Fig. 12. This image was taken using an iodine-based contrast medium added a little. Because the x-ray duration was about 1 μs, the stop-motion image of water could be obtained.

Figures 13 and 14 were obtained by a molybdenum target (Table 2) with a charging voltage of 50 kV and 45 kV, respectively. Figure 13 shows radiograms of concentric-circled steps of 5.0 mm made of PMMA, with a maximum height of 25.0 mm, at a

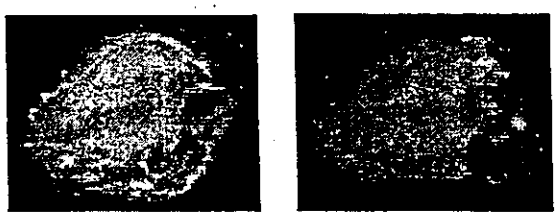

Fig. 15 Angiograms of extracted rabbit hearts.

Fig. 16 Angiogram of an extracted dog heart.

charging voltage of 50 kV. In this radiography, we obtained almost identical contrast images, regardless of whether the 30 μm molybdenum filter was employed or not. An angiogram of the external ear of a rabbit is shown in Fig. 14. The angiography was performed using iodine-based microspheres of 20 μm with a charging voltage of 45 kV, and fine blood vessels of about 50 μm are clearly visible.

Angiography using a cerium target (Table 3) at a charging voltage of 55 kV is shown in Figs. 15 and 16. Figure 15 shows angiograms of hearts extracted from rabbits. These two images were obtained using iodine and cerium microspheres, respectively. Where the cerium spheres were employed, the coronary arteries were barely visible, since cerium spheres transmit the cerium characteristic x-rays easily. In angiography of a larger heart extracted from a dog, using iodine spheres, the coronary arteries were clearly visible (Fig. 16).

5. DISCUSSION

Although photon energy of x-ray lasers has been increased in laboratories around the world, it is difficult to oscillate hard x-ray lasers with energies of 10 keV or higher using ordinary methods. Also, sharp soft x-ray lasers have been produced using a gas-discharge capillary [18-20], the signal to noise (SN) ratio having a lower value assuming that the laser intensity is a signal. As compared with these lasers, the SN ratio of characteristic x-rays generated from weakly ionized plasma is significantly higher if we assume that the characteristic x-ray intensity is signal. In addition, K_β rays can be absorbed by filtering to produce monochromatic K_α rays. In principle, in the characteristic x-ray enhancement by spontaneous emission [21] from weakly ionized linear plasma, coherent x-rays are never produced. However, because the characteristic x-rays from plasma are diffused after passing through two slits, this diffusive mechanism must be solved. Recently, several different x-ray lenses have been developed, and a polycapillary plate [22] is quite useful in order to perform parallel radiography and to realize low-priced x-ray systems. Therefore, we plan to perform quasi-monochromatic parallel radiography in conjunction with this generator. In addition, the refractivity of these sharp x-rays, because of diffusive characteristics, is a matter of great interest.

ACKNOWLEDGEMENTS

This work was supported by Grants-in-Aid for Scientific Research from MECSST (12670902, 13470154, and 13877114), Grants from JST (Test of Fostering Potential), NEDO, and MHLW (HLSRG, RAMT-nano-001, RHGTEFB-genome-005, and RGCD 13C-1).

REFERENCES

[1] Mori H, Hyodo K, Tanaka E, et al.: Small-vessel radiography in situ with monochromatic synchrotron radiation, Radiology, 201, 173-177, 1996.

[2] Davis TJ, Gao D, Gureyev TE, et al.: Phase-contrast imagimg of weakly absorbing materials using hard x-rays, Nature, 373, 595-597, 1995.

[3] Momose A, Takeda T, Itai Y, et al.: Phase-contrast x-ray computed tomography for observing biological soft tissues, Nature Medicine, 2(4), 473-475, 1996.

[4] Sato E, Isobe H, Hoshino F: High intensity flash x-ray apparatus for biomedical radiography. Rev. Sci. Instrum., 57, 1399-1408, 1986.

[5] Sato E, Kimura S, Kawasaki S, et al.: Repetitive flash x-ray generator utilizing a simple diode with a new type of energy-selective function, Rev. Sci. Instrum., 61, 2343-2348, 1990.

[6] Kimura S, Sato E, Sagae M, et al.: Disk-cathode flash x-ray tube driven by a repetitive two-stage Marx pulser, Med. & Biol. Eng. & Comput., 31, S37-S43, 1993.

[7] Sato E, Sagae M, Takahashi K, et al.: High-speed soft x-ray generators in biomedicine, SPIE, 2513, 649-667, 1994.

[8] Sato E, Sagae M, Takahashi K, et al.: Dual energy flash x-ray generator, SPIE, 2513, 723-735, 1994.

[9] Shikoda A, Sato E, Sagae M, et al.: Repetitive flash x-ray generator having a high-durability diode driven by a two-cable-type line pulser, Rev. Sci. Instrum., 65, 850-856, 1994.

[10] Sato E, Takahashi K, Sagae M, et al.: Sub-kilohertz flash x-ray generator utilizing a glass-enclosed cold-cathode triode, Med. & Biol. Eng. & Comput., 32, 289-294, 1994.

[11] Takahashi K, Sato E, Sagae M, et al.: Fundamental study on a long-duration flash x-ray generator with a surface-discharge triode, Jpn. J. Appl. Phys., 33, 4146-4151, 1994.

[12] Sato E, Sagae M, Shikoda A, et al.: High-speed soft x-ray techniques, SPIE, 2869, 937-955, 1996.

[13] Sato E, Sagae M, Ichimaru T, et al.: Tentative study on x-ray enhancement by fluorescent emission of radiation by plasma x-ray source, SPIE, 3771, 51-60, 1999.

[14] Sato E, Hayasi Y, Ichimaru T, et al.: Tentative study on high-photon-energy quasi-x-ray laser generator by forming plasma x-ray source, SPIE, 4183, 326-338, 2000.

[15] Sato E, Suzuki Y, Hayashi Y, et al.: High-intensity quasi-monochromatic x-ray irradiation from the linear plasma target, SPIE, 4505, 154-164, 2001.

[16] Sato E, Hayasi Y, Tanaka E, et al.: Quasi-monochromatic radiography using a high-intensity quasi-x-ray laser generator, SPIE, 4682, 538-548, 2002.

[17] Sato E, Sato K, Tamakawa Y, et al.: Film-less computed radiography system for high-speed Imaging. Ann. Rep. Iwate Med. Univ. Sch. Lib. Arts & Sci., 35, 13-23, 2000.

[18] Rocca JJ, Shlyaptsev V, Tomasel FG, et al.: Demonstration of a discharge pumped table-top soft x-ray laser, Phys. Lev. Lett., 73, 2192-2195, 1994.

[19] Collins G.P: Tabletop capillary-discharge soft-x-ray laser demonstrated, Physics Today, Oct, 19-21, 1994.

[20] Rocca JJG, Chilla JLA, Sakadzic S, et al.: Advances in capillary discharge soft x-ray laser research, SPIE, 4505, 1-6, 2001.

[21] Nakamori N, Yamano K, Yamada M, et al.: Calculation of characteristic x-rays in diagnostic x-ray spectrum, Jpn. J. Appl. Phys., 33, 347-352, 1994.

[22] Sato E, Toriyabe H, Hayasi Y, et al.: Fundamental study on parallel beam radiography using a polycapillary plate, SPIE, 4682, 298-310, 2002.

研 究 論 文

Irradiation of intense characteristic x-rays from weakly ionized linear molybdenum plasma

Eiichi Sato[1)*], Yasuomi Hayasi[1)], Rudolf Germer[2)], Etsuro Tanaka[3)], Hidezo Mori[4)], Toshiaki Kawai[5)], Haruo Obara[6)], Toshio Ichimaru[7)], Kazuyoshi Takayama[8)], Hideaki Ido[9)]

[1)] *Department of Physics, Iwate Medical University*
[2)] *ITP, FHTW FB1 and TU-Berlin*
[3)] *Department of Physiology, School of Medicine, Tokai University*
[4)] *Department of Cardiac Physiology, National Cardiovascular Center Research Institute*
[5)] *Electron Tube Division 2, Hamamatsu Photonics Inc.*
[6)] *Department of Radiological Technology, College of Medical Science, Tohoku University*
[7)] *Department of Radiological Technology, School of Health Sciences, Hirosaki University*
[8)] *Shock Wave Research Center, Institute of Fluid Science, Tohoku University*
[9)] *Department of Applied Physics, Faculty of Engineering, Tohoku Gakuin University*

Research Code No: 204.1
Key Words: flash x-ray, characteristic x-ray, quasi-monochromatic radiography, weakly ionized plasma, linear plasma

Abstract

In the plasma flash x-ray generator, a high-voltage main condenser of approximately 200 nF is charged up to 55 kV by a power supply, and electric charges in the condenser are discharged to an x-ray tube after triggering the cathode electrode. The flash x-rays are then produced. The x-ray tube is a demountable triode that is connected to a turbo molecular pump with a pressure of approximately 1 mPa. As electron flows from the cathode electrode are roughly converged to a rod molybdenum target of 2.0 mm in diameter by the electric field in the x-ray tube, weakly ionized linear plasma, which consists of molybdenum ions and electrons, forms by target evaporation. At a charging voltage of 55 kV, the maximum tube voltage was almost equal to the charging voltage of the main condenser, and the peak current was about 20 kA. When the

* 岩手医科大学教養部物理学科〔〒020-0015 岩手県盛岡市本町通3-16-1〕: Department of Physics. Iwate Medical University
e-mail : dresato@iwate-med.ac.jp

charging voltage was increased, the linear plasma formed, and the K-series characteristic x-ray intensities increased. The K lines were quite sharp and intense, and hardly any bremsstrahlung rays were detected. The x-ray pulse widths were approximately 700 ns, and the time-integrated x-ray intensity had a value of approximately 35 μC/kg at 1.0 m from the x-ray source with a charging voltage of 50 kV.

Received Apr.9, 2003; revision accepted May.9, 2003

1. Introduction

Flash x-rays are a powerful tool for visualizing the inside of high-speed opaque objects, and the maximum photon energy has been increased to roughly 1 MeV in cases where Marx type high-voltage pulse generators are employed[1-3]. On the other hand, several different flash x-ray generators with energies of lower than 150 keV have been developed in order to perform soft radiographies with biomedical applications[4-12], and these generators have large capacity condensers in order to increase x-ray intensity by increasing electrostatic energy.

Recently, soft x-ray lasers have been produced by a gas-discharge capillary[13-16] to form linear plasma, in which laser intensity increases with corresponding increases in capillary length. However, it is quite difficult to increase the laser photon energy beyond 10 keV by light amplification by stimulated emission.

In light enhancement by spontaneous emission, characteristic x-rays are increased[17] in a thick solid target by conversion of bremsstrahlung x-rays into fluorescent x-rays without considering x-ray coherence. Then, by forming the weakly ionized linear plasma using a plate target[18,19], we confirmed irradiation of intense K-series characteristic x-rays from the plasma axial direction, and K-fluorescent yield in proportion to conversion efficiency increased with increases in atomic number.

In this paper, we describe a flash x-ray generator utilizing a rod-target radiation tube, which we used to perform a preliminary experiment for generating intense quasi-monochromatic x-rays by forming a linear molybdenum plasma cloud around a fine target.

2. Generator

2.1 High-voltage circuit

Figure 1 shows a block diagram of the high-intensity plasma flash x-ray generator. This generator consists of the following essential components: a high-voltage power supply, a high-voltage condenser with a capacity of approximately 200 nF, a turbo-molecular vacuum pump, a krytron pulse generator as a trigger device, and a flash x-ray tube. In this generator, a low-impedance transmission line is em-

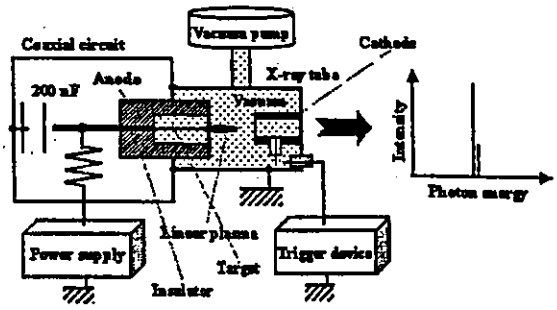

Fig. 1. Block diagram of the high-intensity plasma flash x-ray generator.

ployed in order to increase maximum tube current. The high-voltage main condenser is charged to 55 kV by the power supply, and electric charges in the condenser are discharged to the tube after triggering the cathode electrode with the trigger device. The plasma flash x-rays are then produced.

2.2 X-ray tube

The x-ray tube is a demountable cold cathode triode that is connected to the turbo-molecular pump with a pressure of approximately 1 mPa (Fig. 2). This tube consists of the following major parts: a pipe-shaped carbon cathode with a bore diameter of 10.0 mm, a trigger electrode made from copper wire, a stainless steel vacuum chamber, a nylon insulator, a polyethylene terephthalate polyester film (Mylar) x-ray window 0.25 mm in thickness, and a rod-shaped molybdenum target 2.0 mm in diameter with a tip angle of 60°. The distance between the anode and cathode electrodes is approximately 20 mm, and the trigger electrode is set in the cathode electrode. As electron beams from the cathode electrode are roughly converged to the target by the electric field in the tube, evaporation leads to the formation of a weakly ionized linear plasma, consisting of molybdenum ions and electrons, around the fine target.

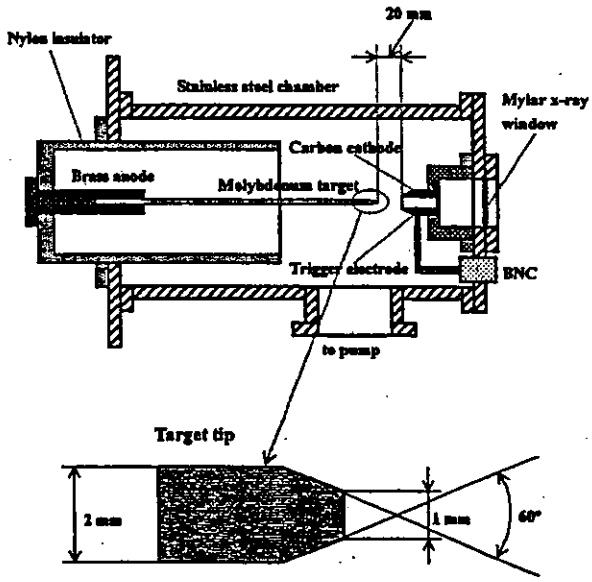

Fig. 2. Schematic drawing of the flash x-ray tube with a rod target.

2.3 Principle of characteristic x-ray irradiation

In the linear plasma, bremsstrahlung photons with energies higher than the K-absorption edge are effectively absorbed and are converted into fluorescent x-rays (Fig. 3). The plasma then transmits the fluorescent rays easily, and bremsstrahlung rays with energies lower than the K-edge are also absorbed by the plasma. In addition, because bremsstrahlung rays are not emitted in the direction opposite that of electron acceleration, intense characteristic x-rays are generated from the plasma-axial direction.

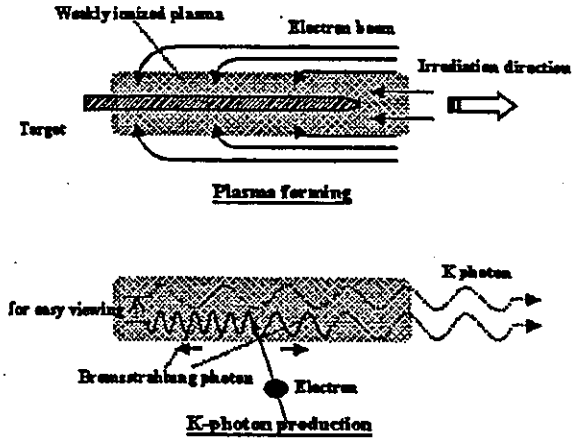

Fig. 3. K-photon irradiation from the plasma.

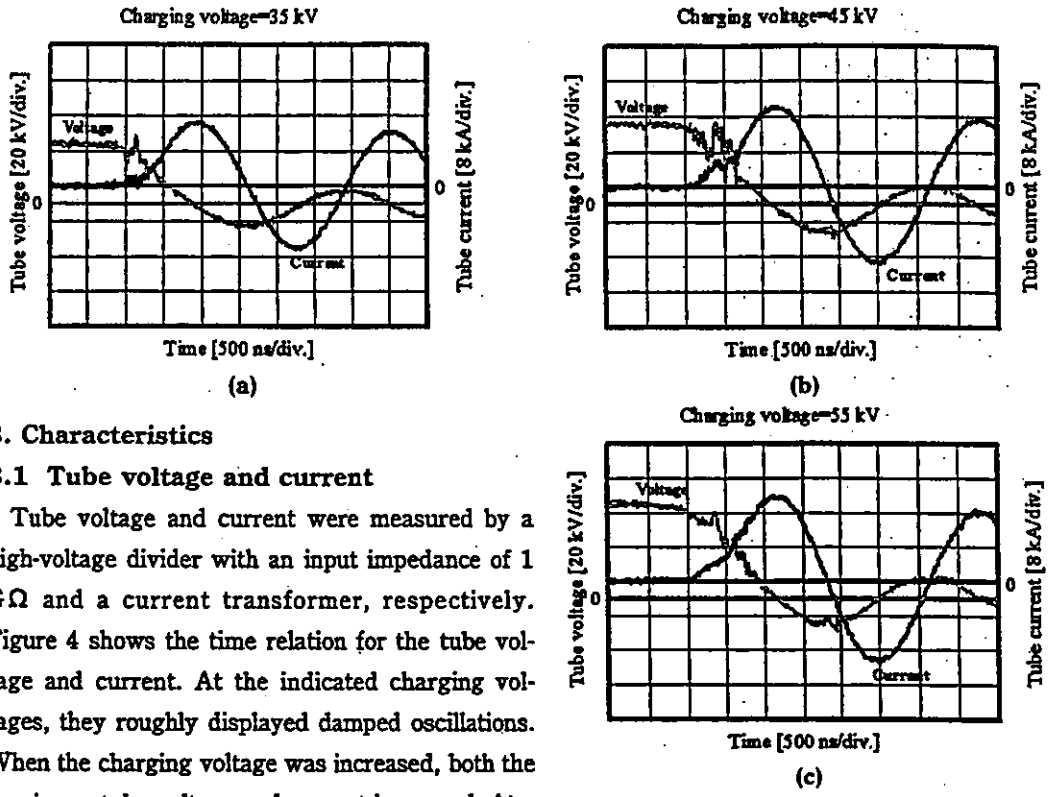

Fig. 4. Tube voltages and currents with a charging voltage of (a) 35 kV, (b) 45 kV, and (c) 55 kV.

3. Characteristics

3.1 Tube voltage and current

Tube voltage and current were measured by a high-voltage divider with an input impedance of 1 GΩ and a current transformer, respectively. Figure 4 shows the time relation for the tube voltage and current. At the indicated charging voltages, they roughly displayed damped oscillations. When the charging voltage was increased, both the maximum tube voltage and current increased. At a charging voltage of 55 kV, the maximum tube voltage was almost equal to the charging voltage of the main condenser, and the maximum tube current was approximately 20 kA.

3.2 X-ray output

X-ray output pulse was detected using a combination of a plastic scintillator and a photomultiplier (Fig. 5). The x-ray pulse height substantially increased with corresponding increases in the charging voltage, but there was a big decrease when a monochromatic molybdenum filter of 30μm in thickness was inserted. The x-ray pulse widths were about 700 ns, and the time-integrated x-ray intensity measured by a thermoluminescence dosimeter (Kyokko TLD Reader 1500 having MSO-R elements without energy compensation) had a value of about 35μC/kg at 1.0 m from the x-ray source with a charging voltage of 50 kV.

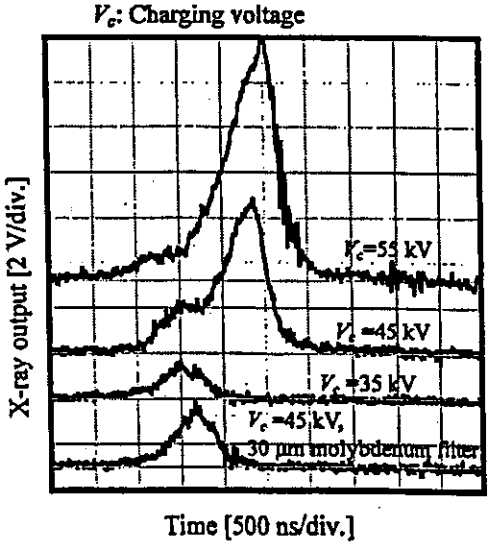

Fig. 5. X-ray outputs at the indicated conditions.

3.3 X-ray source

In order to measure images of the plasma x-ray source, we employed a pinhole camera with a hole diameter of 100μm (Fig. 6). When the charging voltage was increased, the plasma x-ray source grew, and both spot dimension and intensity increased. In contrast, both the dimension and intensity decreased upon insertion of the monochromatic filter.

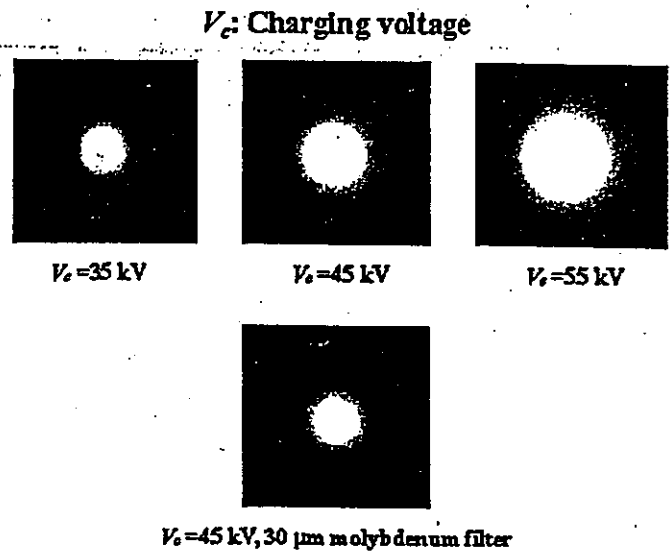

Fig. 6. Images of the plasma x-ray source.

3.4 X-ray spectra

X-ray spectra from the plasma source were measured by a transmission-type spectrometer[19] (Fig. 7) with a lithium fluoride curved crystal 0.5 mm in thickness. The spectra were taken by a computed radiography (CR) system (Konica Regius 150)[20] with a wide dynamic range, and relative x-ray intensity was calculated from Dicom digital data. Figure 8 shows measured spectra from the molybdenum target. In fact, we observed quite sharp lines of K-series characteristic x-rays such as lasers, while bremsstrahlung rays were hardly detected. The characteristic x-ray intensity substantially increased with corresponding increases in the charging voltage and decreased with insertion of the filter.

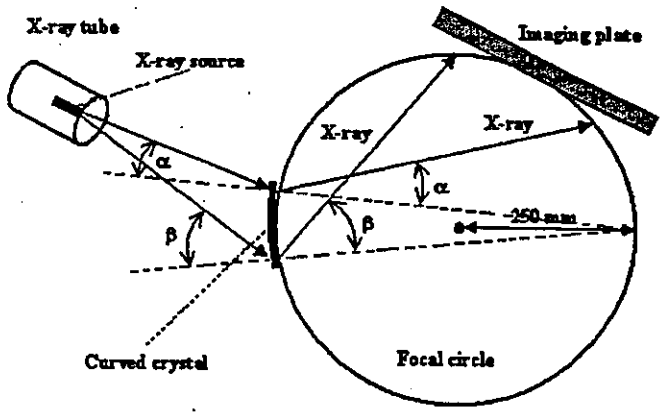

Fig. 7. Transmission-type spectrometer using an imaging plate.

3.5 X-ray divergence by slits

In order to ascertain the difference in characteristics between x-rays from a conventional tube and these from the plasma tube, we employed two lead slits in order to measure the divergence of the x-rays (Fig. 9). As compared with incoherent x-rays from a conventional tube with a tungsten target, the characteristic x-rays from the linear plasma were diffused greatly after passing through the two slits (Fig. 10).

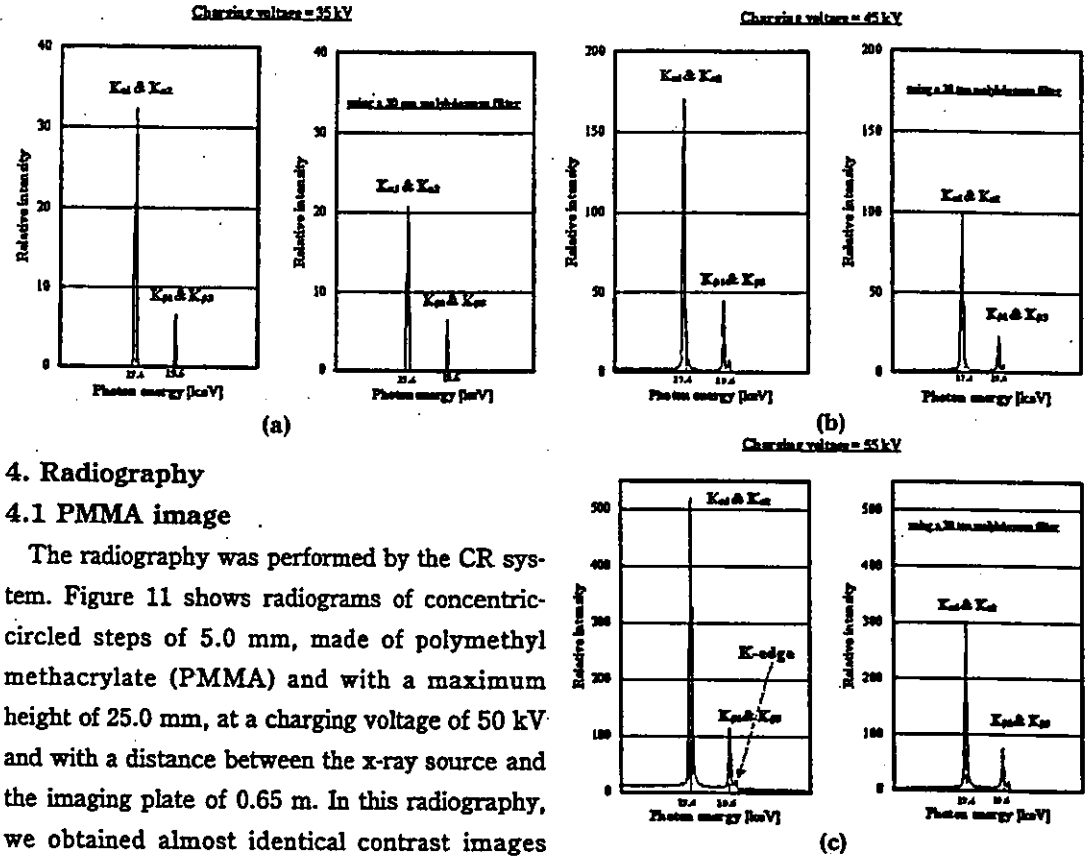

Fig. 8 X-ray spectra from weakly ionized molybdenum plasma with a charging voltage of (a) 35 kV, (b) 45 kV, and (c) 55 kV.

4. Radiography

4.1 PMMA image

The radiography was performed by the CR system. Figure 11 shows radiograms of concentric-circled steps of 5.0 mm, made of polymethyl methacrylate (PMMA) and with a maximum height of 25.0 mm, at a charging voltage of 50 kV and with a distance between the x-ray source and the imaging plate of 0.65 m. In this radiography, we obtained almost identical contrast images regardless of whether the 30μm-thick molybdenum filter was employed or not. The image qualities of radiograms taken by the plasma generator were somewhat soft compared with a radiogram obtained by a conventional molybdenum x-ray tube for mammography, using the filter, with a tube voltage of 25 kV and the same distance between the x-ray source and the imaging plate.

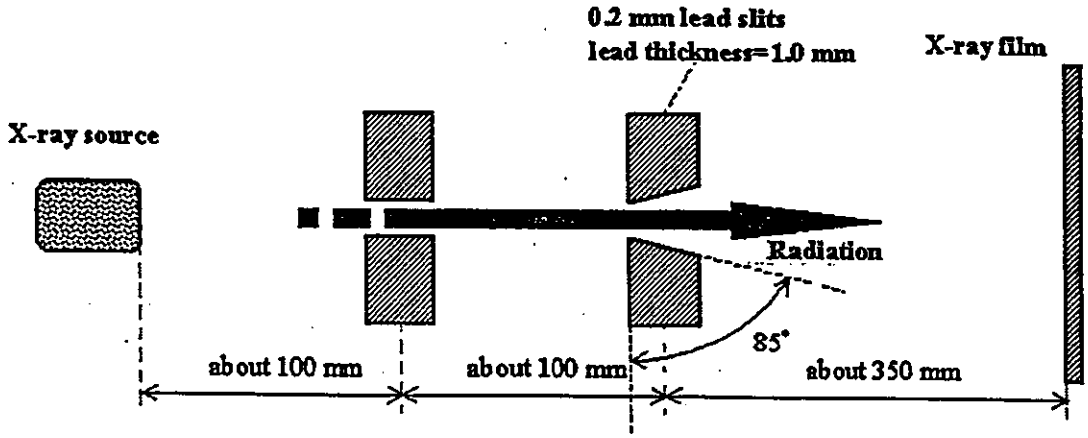

Fig. 9. Experimental setup for measuring x-ray divergence using two lead slits.

4.2 Image resolution and applications

Firstly, rough measurements of image resolution were made using wires. Figure 12 shows radiograms of tungsten wires coiled around rods made of PMMA with a charging voltage of 50 kV. Although the image contrast increased with increases in the wire diameter, a 50μm-diameter wire could be observed.

The image of water droplets falling into a polypropylene beaker from an injector is shown in Fig. 13. This image was taken with a charging voltage of 45 kV, with the slight addition of an iodine-based contrast medium. Because the x-ray duration was about 1μs, the stop-motion image of water could be obtained.

Figure 14 shows an angiogram of the external ear of a rabbit; iodine-based microspheres of 20μm diameter were used with a charging voltage of 45 kV, and fine blood vessels of about 50μm were clearly visible. In angiography of an extracted rabbit heart using iodine spheres with a voltage of 55 kV, fine coronary arteries were observed in the enlarged image (Fig. 15).

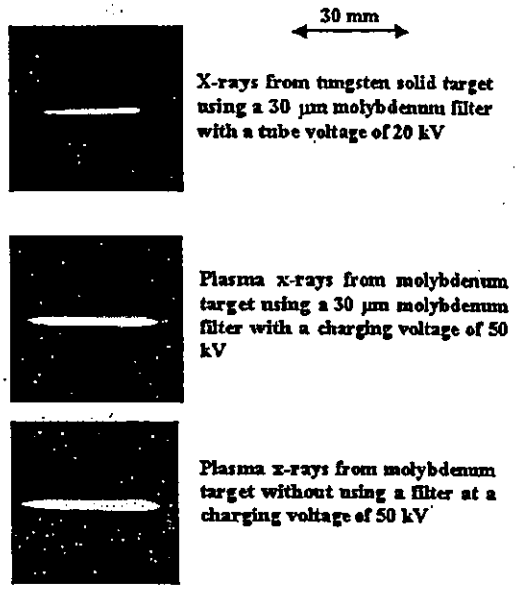

Fig. 10. X-ray divergence with two lead slits.

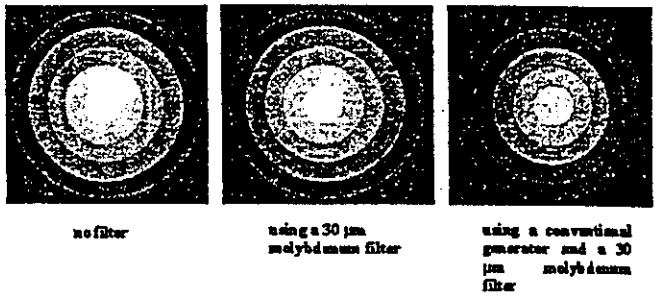

Fig. 11. Radiograms of concentric-circled steps of 5.0 mm with a maximum height of 25.0 mm at the indicated conditions.

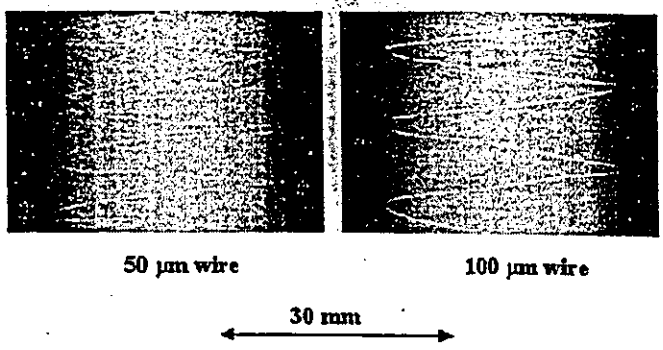

Fig. 12. Radiograms of tungsten wires of 50 and 100μm in diameter coiled around rods made of polymethyl methacrylate.

5. Discussion

Concerning the spectrum measurement, we obtained quite intense and sharp K-series lines by forming a weakly ionized linear plasma x-ray source. In fact, these rays penetrated the molybdenum filter easily and were diffused after passing through slits, with the average linear absorption coefficient slightly larger than that for quasi-monochromatic x-rays

from the solid molybdenum target. In the former experiment concerning the slit divergence, the radiations from linear plasma formed by a capillary were also diffused greatly as compared with incoherent visible light beams[21].

In this research, we obtained sufficient characteristic x-ray intensity per pulse for CR radiography without using a monochromatic filter, and the generator produced high-dose-rate quasi-monochromatic x-rays in a quantity roughly 1,000 times greater than the synchrotron monochromatic x-rays. In addition, since the photon energy of characteristic x-rays can be controlled by changing target elements, various quasi-monochromatic high-speed radiographies, such as high-contrast micro angiography[22] and parallel radiography[23] using an x-ray lens, will be possible.

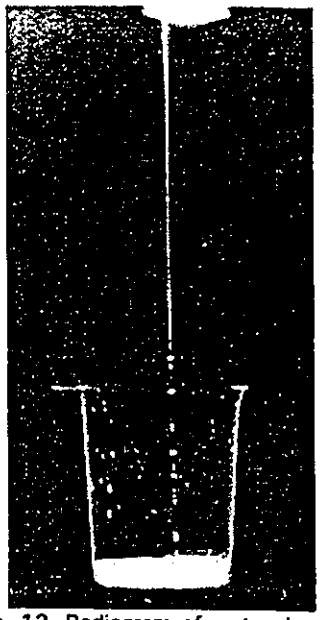

Fig. 13. Radiogram of water droplets falling into a polypropylene beaker from an injector.

Acknowledgment

This work was supported by Grants-in-Aid for Scientific Research from MECSST (12670902, 13470154, and 13877114), Grants from JST (Test of Fostering Potential), NEDO, and MHLW (HLSRG, RAMT-nano-001, RHGTEFB-genome-005, and RGCD13C-1).

References

1) Mattsson A: Some characteristics of a 600 kV flash x-ray tube. Physica Scripta 5: 99-102, 1972
2) Germer R: X-ray flash techniques. J Phys E: Sci Instrum 12: 336-350, 1979
3) Sato E, Kimura S, Kawasaki S, et al.: Repetitive flash x-ray generator utilizing a simple diode with a new type of energy-selective function. Rev Sci Instrum 61: 2343-2348, 1990
4) Sato E, Isobe H, Hoshino F: High intensity flash x-ray apparatus for biomedical radiography. Rev Sci Instrum 57: 1399-1408, 1986

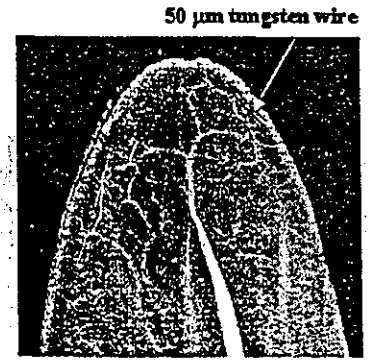

Fig. 14. Angiograms of the external ear of a rabbit.

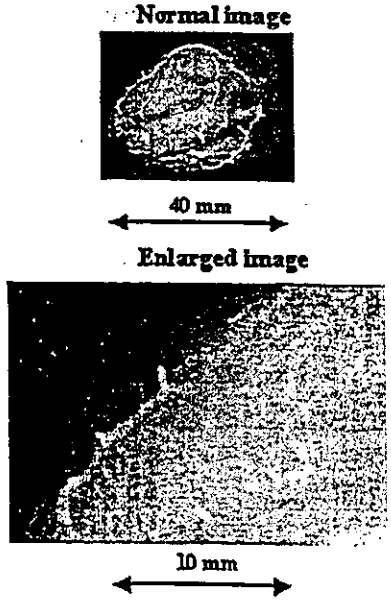

Fig. 15. Angiograms of an extracted rabbit heart.

5) Sato E, Shikoda A, Kimura S, et al.: Repetitive compact flash x-ray generators for soft radiography. SPIE 1801: 628-642, 1992
6) Kimura S, Sato E, Sagae M, et al.: Disk-cathode flash x-ray tube driven by a repetitive two-stage Marx pulser. Med & Biol Eng & Comput 31: S37-S43, 1993
7) Sato E, Sagae M, Takahashi K, et al.: High-speed soft x-ray generators in biomedicine. SPIE 2513: 649-667, 1994
8) Sato E, Sagae M, Takahashi K, et al.: Dual energy flash x-ray generator. SPIE 2513: 723-735, 1994
9) Shikoda A, Sato E, Sagae M, et al.: Repetitive flash x-ray generator having a high-durability diode driven by a two-cable-type line pulser. Rev Sci Instrum 65: 850-856, 1994
10) Sato E, Takahashi K, Sagae M, et al.: Sub-kilohertz flash x-ray generator utilizing a glass-enclosed cold-cathode triode. Med & Biol Eng & Comput 32: 289-294, 1994
11) Takahashi K, Sato E, Sagae M, et al.: Fundamental study on a long-duration flash x-ray generator with a surface-discharge triode. Jpn J Appl Phys 33: 4146-4151, 1994
12) Sato E, Sagae M, Shikoda A, et al.: High-speed soft x-ray techniques. SPIE 2869: 937-955, 1996
13) Rocca JJ, Shlyaptsev V, Tomasel FG, et al.: Demonstration of a discharge pumped table-top soft x-ray laser. Phys Lev Lett 73: 2192-2195, 1994
14) Collins GP: Tabletop capillary-discharge soft-x-ray laser demonstrated. Physics Today Oct: 19-21, 1994
15) Rocca JJG, Chilla JLA, Sakadzic S, et al.: Advances in capillary discharge soft x-ray laser research. SPIE 4505: 1-6, 2001
16) Le Pape S, Zeitoun Ph, Rocca JJG, et al.: Characterisation of an x-ray laser beam. SPIE 4505: 23-34, 2001
17) Nakamori N, Yamano K, Yamada M, et al.: Calculation of characteristic x-rays in diagnostic x-ray spectrum. Jpn J Appl Phys 33: 347-352, 1994
18) Sato E, Sagae M, Ichimaru T, et al.: Tentative study on x-ray enhancement by fluorescent emission of radiation by plasma x-ray source. SPIE 3771: 51-60, 1999
19) Sato E, Hayashi Y, Ichimaru T, et al.: Tentative study on high-photon-energy quasi-x-ray laser generator by forming plasma x-ray source. SPIE 4183: 326-338, 2000
20) Sato E, Sato K, Tamakawa Y, et al.: Film-less computed radiography system for high-speed Imaging. Ann Rep Iwate Med Univ Sch Lib Arts & Sci 35: 13-23, 2000
21) Sato E, Hayashi Y, Usuki T, et al.: Characteristics of a capillary-discharge flash x-ray generator. SPIE 4786: 173-182, 2002
22) Mori H, Hyodo K, Tanaka E, et al.: Small-vessel radiography in situ with monochromatic synchrotron radiation. Radiology 201: 173-177, 1996
23) Sato E, Komatsu M, Hayashi Y, et al.: Quasi-monochromatic parallel radiography achieved with a plane-focus x-ray tube. SPIE 4786: 151-161, 2002

Available online at www.sciencedirect.com
SCIENCE DIRECT®
Neurochemistry International 43 (2003) 573–580
NEUROCHEMISTRY International
www.elsevier.com/locate/neuint

In vivo monitoring of norepinephrine and its metabolites in skeletal muscle

Noriyuki Tokunaga [a], Toji Yamazaki [a,*], Tsuyoshi Akiyama [a], Shunji Sano [b], Hidezo Mori [a]

[a] *Department of Cardiac Physiology, National Cardiovascular Center Research Institute, 5-7-1 Fujishiro-dai, Suita, Osaka 565-8565, Japan*
[b] *Department of Cardiovascular Surgery, Okayama University Medical School, Okayama 700-8558, Japan*

Received 2 October 2002; accepted 10 January 2003

Abstract

Although skeletal muscle sympathetic nerve activity plays an important role in the regulation of vascular tone and glucose metabolism, relatively little is known about regional norepinephrine (NE) kinetics in the skeletal muscle. With use of the dialysis technique, we implanted dialysis probes in the adductor muscle of anesthetized rabbits and examined whether dialysate NE and its metabolites were influenced by local administration of pharmacological agents through the dialysis probes. Dialysate dihydroxyphenylglycol (DHPG) and 3-methoxy-4-hydroxyphenylglycol (MHPG) were measured as two major metabolites of NE. The skeletal muscle dialysate NE, DHPG and MHPG were 11.7 ± 1.2, 38.1 ± 3.2, and 266.1 ± 28.7 pg/ml, respectively. Basal dialysate NE levels were suppressed by tetrodotoxin (Na^+ channel blocker, 10 μM) (5.1 ± 0.6 pg/ml), and augmented by desipramine (NE uptake blocker, 100 μM) (25.8 ± 3.2 pg/ml). Basal dialysate DHPG levels were suppressed by pargyline (monoamine oxidase blocker, 1 mM) (24.3 ± 4.6 pg/ml) and augmented by reserpine (vesicle NE transport blocker, 10 μM) (75.8 ± 2.7 pg/ml). Basal dialysate MHPG levels were not affected by pargyline, reserpine, or desipramine. Addition of tyramine (sympathomimetic amine, 600 μM), KCl (100 mM), and ouabain (Na^+–K^+ ATPase blocker, 100 μM) caused brisk increases in dialysate NE levels (200.9 ± 14.2, 90.6 ± 25.7, 285.3 ± 46.8 pg/ml, respectively). Furthermore, increases in basal dialysate NE levels were correlated with locally administered desipramine (10, 100 μM). Thus, dialysate NE and its metabolite were affected by local administration of pharmacological agents that modified sympathetic nerve endings function in the skeletal muscle. Skeletal muscle microdialysis with local administration of a pharmacological agent provides information about NE release, uptake, vesicle uptake and degradation at skeletal muscle sympathetic nerve endings.

Keywords: Dihydroxyphenylglycol; 3-Methoxy-4-hydroxyphenylglycol; Microdialysis; Rabbit; Skeletal muscle

1. Introduction

Muscle sympathetic nerve activity exerts an important action on the regulation of vascular tone (Lundvall and Edfeldt, 1994) and glucose metabolism (Fagius and Berne, 1994; Spraul et al., 1994) in the skeletal muscle. Clinical and experimental studies suggest that alterations of sympathetic nerve function at the skeletal muscle are involved in the pathogenesis of various diseases (Cabassi et al., 2001; Grassi et al., 1995). Further, organ-specific norepinephrine (NE) spillover demonstrated that as much as 20% of the norepinephrine entering plasma derives from the skeletal muscle (Esler et al., 1984). Thus, norepinephrine kinetics in the skeletal muscle plays an important role in various physiological and pathophysiological conditions. However, owing to methodological problems, relatively little is known about NE kinetics in the skeletal muscle.

To elucidate NE kinetics at the sympathetic nerve endings, NE release, uptake, vesicle transport, vesicle storing capacity and metabolism should be assessed. Until now, available methodology for examination of nerve endings function has been limited to assessment of radiolabelled-NE kinetics. In practice, this sophisticated technique has provided a powerful method for the analysis of heart (Thompson et al., 1998), kidney (Wallin et al., 1996) and liver (Aneman et al., 1996; Mundinger et al., 1997). However, dispersed organ systems, such as skeletal muscle and skin are not suitable for NE spillover. On the other hand, muscle sympathetic nerve activity was recorded by microneurography (Anderson et al., 1989; Ferguson et al., 1990). This technique provides information only about NE releasing function, while NE uptake, NE metabolism and other functions remain unclear.

Recently microdialysis technique in combination with a high-performance liquid chromatographic method with

* Corresponding author. Tel.: +81-6-6833-5012; fax: +81-6-6872-8092.
E-mail address: yamazaki@ri.ncvc.go.jp (T. Yamazaki).

0197-0186/03/$ – see front matter
doi:10.1016/S0197-0186(03)00064-0

electrochemical detection (HPLC-ED) has offered a unique and powerful method for analysis of NE kinetics in cardiac sympathetic nerve endings (Takauchi et al., 1997; Yamazaki et al., 1995, 1997). This method is suitable for probe-implantable organs, such as heart, kidney (Zou and Cowley, 1997), brain (Kiss et al., 1995) and adipose tissue (Arner et al., 1988). Modification of the analytical conditions for the HPLC-ED system may allow extension of this method to skeletal muscle as well. Measurement of NE and its metabolites in the skeletal muscle could be particularly appropriate to gain information about skeletal muscle-specific sympathetic nerve endings function (Bruce et al., 2002; Gronlund et al., 1991). In the present study, to examine basal NE kinetics at the skeletal muscle sympathetic nerve endings, we performed skeletal muscle dialysis in combination with local administration of various neuropharmacological drugs.

2. Methods

2.1. Animal preparation

Male Japanese white rabbits weighing 2.5–3 kg each were anesthetized with pentobarbital sodium (30–35 mg/kg, i.v.). The level of anesthesia was maintained with a continuous intravenous infusion of pentobarbital sodium (1–2 mg/kg h). The animals were intubated and ventilated with room air mixed with oxygen. Body temperature was maintained with a heated pad and lamp. All protocols were performed in accordance with the American Physiological Society guidelines for the use of animals. An electrocardiogram, heart rate, and arterial blood pressure were simultaneously monitored with a data recorder. After a longitudinal skin incision of left groin was made, the dialysis probes were implanted in the left adductor muscle with a fine guiding needle (Fig. 1). To compare dialysate NE and its metabolites between skeletal and cardiac muscle, in some of the experiments, we implanted a dialysis probe in the left ventricle free wall in the heart.

2.2. Dialysis technique

With the dialysis technique, dialysate NE and its metabolite concentrations were measured as an index of skeletal muscle interstitial levels. For skeletal muscle dialysis, we designed a transverse dialysis probe. The dialysis fiber (13 mm length, 0.31 mm o.d. and 0.2 mm i.d.; PAN-1200, 50,000 molecular mass cut-off, Asahi Chemical, Tokyo, Japan) was glued at both ends into a polyethylene tube (25 cm length, 0.5 mm o.d. and 0.2 mm i.d.) (Akiyama et al., 1991). The dialysis probe was perfused with Ringer solution at a speed of 10 μl/min using a microinjection pump (CMA 102, Carnergie Medicin, Stockholm, Sweden). One sampling period was 10 min (one dialysate sample volume: 100 μl). In the preliminary experiment, we examined the time course of dialysate NE levels at 30–60 min interval over a period of 240 min ($n = 3$). Dialysate NE levels were 21.1 ± 8.0 pg/ml at 30 min after probe implantation, then decreased to 9.0 ± 0.3 pg/ml at 90 min after implantation. Thereafter, it reached an almost steady level at 120–240 min after probe implantation. Therefore, dialysate sampling was started 120 min after probe implantation in the experimental protocol. Each sample was collected in a 300 μl microtube containing 10 μl of 0.1N HCl, to prevent amine oxidation.

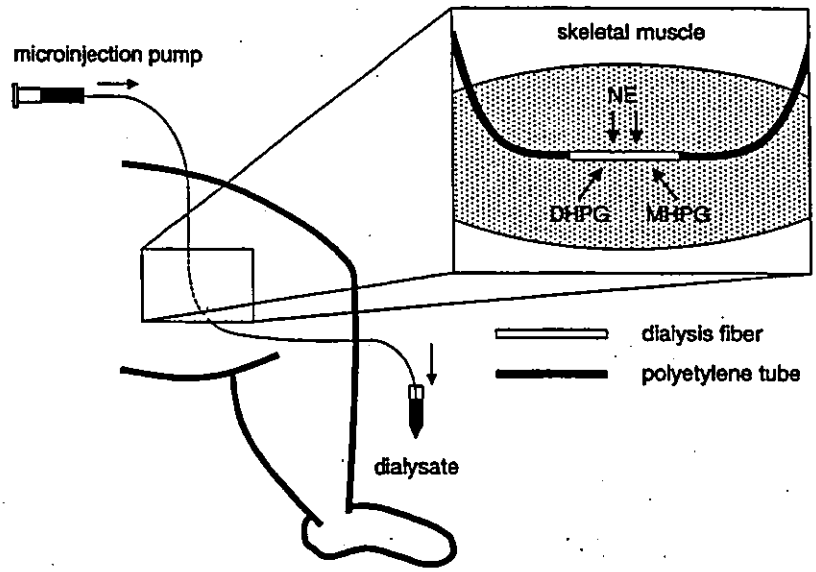

Fig. 1. Dialysis technique in skeletal muscle. Dialysis probe was implanted in adductor muscle with a fine guiding needle and perfused with Ringer solution containing neuropharmacological agents using a microinjection pump. NE: norepinephrine; DHPG: dihydroxyphenylglycol; MHPG: 3-methoxy-4-hydroxyphenylglycol.

2.3. Experimental protocols

In the present study, to examine basal NE kinetics at the skeletal muscle sympathetic nerve endings, we performed skeletal muscle dialysis in combination with local administration of various neuropharmacological drugs. We referred to the previous experiments on the measurement of cardiac dialysate to determine the concentrations of pharmacological agents and sampling time (Akiyama et al., 1991; Yamazaki et al., 1997).

2.3.1. Protocol 1: source of dialysate NE in skeletal muscle

Interstitial NE derived mainly from circulating NE and/or regional sympathetic nerve endings. It is unclear to what extent regional sympathetic nerve endings contribute to change in dialysate NE. To elucidate the source of dialysate NE in the skeletal muscle, we modulated local NE releasing and up-taking function by local administration of a blocking agent. Tetrodotoxin (TTX, NE release blocker, 10 μM) or desipramine (NE uptake blocker: 10, 100 μM) was locally administered through the dialysis probe. Dialysate NE measurement was performed before, 30, and 60 min after the administration.

2.3.2. Protocol 2: influence of neuronal NE release and storage of NE on dialysate NE levels

To examine NE releasing function in skeletal muscle sympathetic nerve endings, we locally administered high K^+ (KCl 100 mM) and ouabain (Na^+–K^+ ATPase blocker, 100 μM) through the dialysis probes, and obtained the dialysate NE responses. Furthermore, to examine storage capacity of NE in skeletal muscle sympathetic nerve endings, we locally administered tyramine (NE releasing sympathomimetic amine, 600 μM) through the dialysis probe (Takauchi et al., 2000). Dialysate NE measurement was performed before, 0–10, and 10–20 min after the administration of KCl or tyramine. In the case of ouabain, to compare the response with the previous studies on cardiac dialysis, one sampling period was set at 15 min and ouabain was locally administered for 60 min (Yamazaki et al., 2001b).

2.3.3. Protocol 3: influence of axoplasmic NE disposition on dialysate dihydroxyphenylglycol (DHPG) levels

The released NE is mainly re-uptaken and mobilized into the stored NE vesicle. Furthermore, axoplasmic NE is partially metabolized with monoamine oxidase (MAO) (Youdim et al., 1988). DHPG is a major metabolite of NE with MAO and served as an index of axoplasmic NE levels (Kopin, 1985). To examine whether dialysate DHPG level reflects axoplasmic NE disposition, we locally administered these neuronal pathway inhibitors and measured dialysate DHPG levels. Pargyline (MAO inhibitor, 1 mM), reserpine (vesicle NE transport inhibitor, 10 μM), or desipramine (100 μM) was separately administered, and dialysate DHPG responses were measured.

2.3.4. Protocol 4: influence of axoplasmic NE disposition on dialysate 3-methoxy-4-hydroxyphenylglycol (MHPG) levels

MHPG is produced by extraneuronal *O*-methylation of DHPG and by the extraneuronal combination of catechol *O*-methyltransferase (COMT) and MAO on NE (Kopin, 1985). We examined the effects of pargyline (1 mM), reserpine (10 μM) and desipramine (100 μM) on dialysate MHPG levels.

2.3.5. Protocol 5: comparison of dialysate NE and its metabolites between cardiac and skeletal muscle

In previous papers, we performed cardiac microdialysis for myocardial interstitial NE and DHPG measurements (Akiyama et al., 1991; Yamazaki et al., 1997). Although the details of measurements have already been reported, whether dialysate NE and its metabolites in cardiac muscle are comparable to those in skeletal muscle remains unclear. We measured dialysate NE and its metabolites in myocardial interstitium in separate rabbits. To compare the results in cardiac and skeletal muscle, the levels of NE and its metabolites in cardiac muscle were corrected by the difference of the in vitro NE recovery rates, and the data were expressed as the level of NE and its metabolites in dialysate.

2.4. Analytical procedure

Half of the dialysate sample was used for the NE measurement, and the remaining sample was split for the DHPG and MHPG measurements. Dialysate NE concentrations were measured by HPLC-ED (Eicom, Japan) after removing interfering compounds by an alumina procedure (Anton and Sayer, 1962). The dialysate DHPG and MHPG were measured directly by two other HPLC-ED. Details of HPLC-ED for NE and DHPG measurements have been described elsewhere (Takauchi et al., 1997; Yamazaki et al., 1995). The dialysate MHPG was measured directly by another HPLC-ED. Separation was performed using an analytical reverse-phase column with a flow of 0.2 ml/min. The amperometric detector was operated at 0.55 V versus an Ag/AgCl reference electrode. The mobile phase consisted of 1-octane-sulfonic sodium salt (200 mg/l final concentration) in 0.1 M phosphate buffer (pH 6.0) and methanol (97:3, v/v). The limit of quantification for MHPG was 900 fg in a 30 μl injection.

2.5. Materials

The following drugs were used: TTX (Wako Pure Chemical Co., Osaka, Japan), desipramine (Sigma), KCl (Wako Pure Chemical), ouabain (Sigma), tyramine (Sigma), pargyline (Sigma), reserpine (Daiichi Pharmaceutical Co., Tokyo, Japan).

At the end of each experiment, the rabbits were killed with an overdose of pentobarbital sodium and the implant sites were checked to confirm that the dialysis probes had

been implanted within the left adductor muscle. Statistical analysis of the data was performed by analysis of variance (ANOVA) followed by Scheffé's F, Dunnett's post-hoc procedure. Paired t-test was applied to analyze the dialysate DHPG levels before and after administration of pharmacological drugs. Statistical significance was defined as $P < 0.05$. Values are presented as mean ± S.E.

3. Results

Hemodynamic variables of arterial pressure and heart rate were unaltered during local administration of the pharmacological agents. Further, no arrhythmia occurred during the experimental study.

3.1. Protocol 1: source of dialysate NE in skeletal muscle

Fig. 2 shows dialysate NE levels before and after local administration of TTX (10 μM) or desipramine (100 μM). Local administration of TTX significantly decreased the dialysate NE levels from 15.4 ± 2.4 to 5.1 ± 0.6 pg/ml at 30 min of administration. This decrease in dialysate NE was preserved at 60 min of administration. Local administration of desipramine significantly increased the dialysate NE levels from 11.1 ± 1.4 to 25.8 ± 3.2 pg/ml at 30 min of administration. This increase was also preserved during the administration. Furthermore, the increase in dialysate NE (18.7 ± 2.9 pg/ml) was observed at 10 μM of desipramine. Increases in dialysate NE levels were correlated with locally administered desipramine (10, 100 μM).

3.2. Protocol 2: influence of neuronal NE release and storage of NE on dialysate NE levels

Fig. 3 shows the time course of local administration of tyramine (600 μM) or KCl (100 mM). Local administration of tyramine significantly increased the dialysate NE levels from 23.9 ± 2.7 to 200.9 ± 14.2 pg/ml. Local administration of KCl significantly increased the dialysate NE levels from 11.7 ± 2.8 pg/ml at control to 84.7 ± 20.8 pg/ml at 10 min, 90.6 ± 25.7 pg/ml at 20 min. Fig. 4 shows the time course of the dialysate NE levels during local administration of ouabain (100 μM). Local administration of ouabain significantly increased the dialysate NE levels from 17.8 ± 2.0 pg/ml at control to 57.2 ± 21.2 pg/ml at 15 min, 206.9 ± 48.3 pg/ml at 30 min, and 285.3 ± 46.8 pg/ml at 45 min. Subsequently, a slow decline occurred but high dialysate levels were maintained during locally applied ouabain.

3.3. Protocol 3: influence of axoplasmic NE disposition on dialysate DHPG levels

Fig. 5 shows dialysate DHPG levels in various conditions. Local administration of pargyline (1 mM) significantly decreased dialysate DHPG levels from 39.4 ± 6.6 pg/ml at control to 24.3 ± 4.6 pg/ml. Local administration of reserpine (10 μM) significantly increased dialysate DHPG levels from 35.0 ± 4.7 to 75.8 ± 2.7 pg/ml. Local administration of desipramine (100 μM) did not affect dialysate DHPG levels.

3.4. Protocol 4: influence of axoplasmic NE disposition on dialysate MHPG levels

Dialysate MHPG levels averaged 212.4 ± 6.5 pg/ml at control. Local administration of pargyline (1 mM), reserpine (10 μM) and desipramine (100 μM) did not affect dialysate MHPG levels (pargyline: 170.7 ± 8.9, reserpine: 247.4 ± 20.5, desipramine 197.5 ± 15.5 pg/ml).

3.5. Protocol 5: comparison of dialysate NE and its metabolites between cardiac and skeletal muscle

Basal cardiac dialysate NE, DHPG, and MHPG levels were 57.3 ± 13.7, 353.1 ± 53.4, and 447.3 ± 64.3 pg/ml, respectively (Table 1). Basal skeletal muscle dialysate NE,

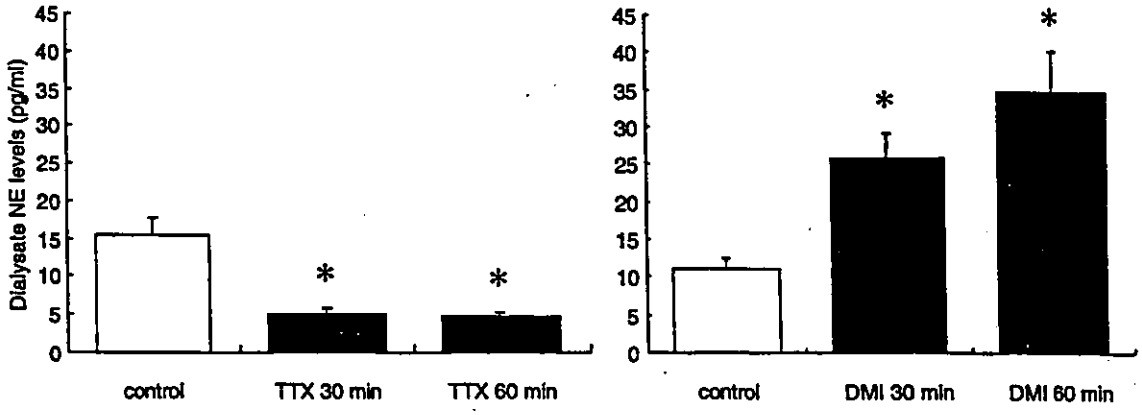

Fig. 2. Local administration of TTX (10 μM) markedly decreased the dialysate NE levels ($n = 7$). In contrast, DMI (100 μM) significantly increased the dialysate NE levels. NE: norepinephrine; TTX: tetrodotoxin; DMI: desipramine. *$P < 0.05$ vs. control.